Fort Lauderdale, Florida, USA
inter-noise 99
1999 December 06-08

PREDICTING THE STATOR VIBRATION SPECTRUM OF INDUCTION MACHINES UNDER NORMAL OPERATION

Koen Delaere, Asmo Tenhunen*, Ward Heylen**, Kay Hameyer, Ronnie Belmans

Esat-Elen Electrical Energy, Kardinaal Mercierlaan 94, B3000 Leuven, Belgium
*Laboratory of Electromechanics, Helsinki University of Technology, PO BOX 3000, 02015 HUT Finland
**Mechanics Dept-PMA, Celestijnenlaan 300B, B3000 Leuven, Belgium

INTRODUCTION

The main electromagnetic source of acoustic noise of induction machines under normal operation are the radial stator vibrations. These vibrations are caused by the radial reluctance forces on the stator teeth due to the magnetic field in the airgap (Maxwell magnetic stress). In order to be able to compute stator deformation, a *local* force expression is needed. Here, a nodal reluctance force expression is derived based upon a coupled magneto-mechanical finite element model. For every relevant rotor position, the magnetic field inside the induction machine is approximated by a time-harmonic solution of the 2D finite element model. The model consists of one quarter of a 4-pole induction machine with external circuits. Using the magnetic field solutions, the force distributions for all relevant rotor positions are computed. At constant rotor speed, the forces are obtained as a function of time. Due to the small slip value under normal operation, a large number of rotor positions need to be considered in order to obtain a periodic sequence suited for a discrete Fourier analysis.

Using a 2D mechanical finite element (FE) model of the induction machine stator, the undamped stator mode shapes are computed taking both iron yoke and copper coils into account. When damping is neglected, the total equation of motion of the stator readily decomposes into the individual modal equations of motion (modal decomposition). The generalized force (*mode participation factor*) acting upon a particular stator mode is found as the correlation between the force distribution and the mode shape. These modal equations of motion are then solved in the frequency domain giving the individual modal spectra. The total vibration spectrum at a specific location on the stator is found by applying the inverse modal decomposition to the modal spectra. The numerically predicted spectra are compared to accelerometer measurements of the vibration spectrum of the stator of a standard induction motor, in order to assess the performance of this 2D method of analysis.

NODAL FORCE EXPRESSION

Both magnetostatic and elasticity FE methods are based upon the minimization of an energy function. The total energy E of the electromechanical system consists of the *elastic energy* U stored in a body with deformation a [1] and the *magnetic energy* W stored in a linear magnetic system with vector potential A [2]:

$$E = U + W = \frac{1}{2} a^T K a + \frac{1}{2} A^T M A, \tag{1}$$

where K is the mechanical stiffness matrix and M is the magnetic 'stiffness' matrix. Considering the similar form of these energy terms, the following system of equations represents the numerically coupled magneto-mechanical system:

$$\begin{bmatrix} M & D \\ C & K \end{bmatrix} \begin{bmatrix} A \\ a \end{bmatrix} = \begin{bmatrix} T \\ R \end{bmatrix}, \tag{2}$$

Table 1: Main properties of the induction machine

analysis parameters	
number of pole pairs	$p = 2$
number of rotor bars	$N_r = 36$
number of stator slots	$N_s = 48$
airgap length	$\delta = 0.905$ mm
outer diameter rotor	109.13 mm
outer diameter iron yoke	167.50 mm
iron yoke length	280 mm
rotor speed	$n = 1478$ rpm
rotor slip	$s = 1.467$ %
rated properties	
mechanical power	$P = 45$ kW
stator current	$I = 81$ A
stator voltage	$V = 400$ V

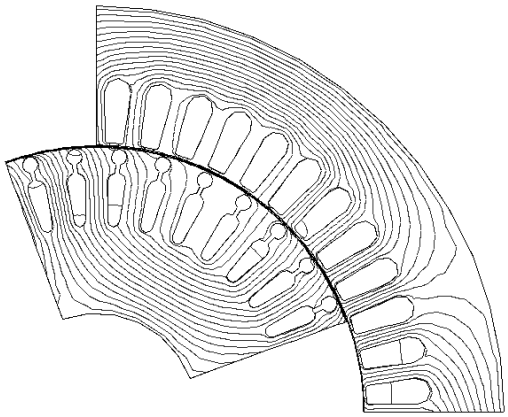

Fig.1 Magnetic field inside the induction machine for rotor position α=20º.

where T is the magnetic source term vector and R represents external forces other than those of electromagnetic origin. Setting the partial derivatives of total energy E with respect to the unknowns $[A \;\; a]^T$ to zero, the combined system (2) with T=0, R=0 is retrieved:

$$\frac{\partial E}{\partial A} = M\,A + \frac{1}{2} a^T \frac{\partial K(A)}{\partial A} a = 0\,, \tag{3}$$

$$\frac{\partial E}{\partial a} = K\,a + \frac{1}{2} A^T \frac{\partial M(a)}{\partial a} A = 0\,. \tag{4}$$

The coupling term D represents magnetostrictive effects and is not considered here, so that D=0 and T=MA. The coupling term C is related to the electromagnetic force: rearranging the mechanical equation (4) into

$$K\,a = -\frac{1}{2} A^T \frac{\partial M(a)}{\partial a} A = -C\,A = F_{em}\,, \tag{5}$$

reveals a means to calculate the forces F_{em} internal to the magneto-mechanical system. These reluctance forces are computed from vector potential A and the *partial derivative* of the magnetic stiffness matrix M with respect to deformation a. The forces F_{em} are also found by applying the virtual work principle to the magnetic energy W for a virtual displacement a [3][4]:

$$F_{em} = -\frac{\partial W}{\partial a} = -\frac{\partial}{\partial a}\left[\frac{1}{2} A^T M(a) A\right], \tag{6}$$

where the vector potential A has to remain unchanged (constant flux) [5]. For the non-linear case, the matrix M is a function of magnetic field and displacement: $M(A,a)$. The magnetic energy W is now given by the integral

$$W = \int_0^A T^{\mathrm{T}}\, dA = \int_0^A A^T M\, dA\,, \tag{7}$$

where T=MA and M^{T}=M is used. The force expression (6) now becomes

$$F_{em} = -\frac{\partial W}{\partial a} = -\int_0^A A^{\mathrm{T}} \frac{\partial M(A,a)}{\partial a} dA\,. \tag{8}$$

The partial derivative $\partial M/\partial a$ is derived explicitly using the analytical shape functions and the magnetization characteristic of the material, e.g. $\nu(B^2)$. Once the vector potential solution A is obtained, the electromagnetic force F_{em} is found using (8).

Table 1 lists the main properties of the standard induction machine. Fig.1 shows the geometry of the magnetic finite element quarter-model of the machine and the magnetic field solution for rotor position α=20º. Fig.2 shows the corresponding force distribution computed using the non-linear force expression (8). The maximum flux density in the teeth is B_{max}=1.43 T. The stator geometry shown in Fig.2 is that of the mechanical 2D finite

element model. The mechanical finite element mesh, used only to compute the stator mode shapes, need not be as dense as the magnetic mesh.

MODE PARTICIPATION FACTORS

Using the 2D mechanical stiffness matrix K and mass matrix M_m, the undamped 2D stator mode shapes are found, some of which are shown in Fig.3. The modes are calculated taking mass and stiffness of the yoke iron and the stator coil copper into account. The machine mounting was not considered for calculating the mode shapes, since in practice the machine mounting is far from rigid, as illustrated further-on.

For a given force pattern f^{α}, occurring for rotor position α, and a given mode shape ϕ_i, the mode participation factor Γ_i^{α} is defined as [6]:

$$\Gamma_i^{\alpha} = \frac{\phi_i{}^T f^{\alpha}}{\phi_i{}^T M_m \phi_i} . \tag{9}$$

The j^{th} element of the vector ϕ_i is the displacement of the i^{th} mode shape at the j^{th} node, while the j^{th} element of the vector f^{α} is the force on the j^{th} node due to the magnetic field for rotor position α.

Fig.4 shows the mode participation factors (MPF) of several modes for rotor positions from 0° to 360°, calculated in 2º steps. The MPF's usually contain both a DC- and an AC-component. Mode 8 has an almost constant MPF of approximately –650, corresponding to an almost constant generalized force wanting to 'collapse' the stator. The DC-components of the MPF's lead to some shrinking of the stator, but no vibrations are produced; only the AC-components of the MPF's give rise to vibrations.

PERIODICITY

In a 4-pole *synchronous* machine, the MPF's have a period of exactly 90º rotor displacement, so 45 field solutions are required to achieve 2° rotor displacement samples. In this 4-pole *induction* machine however, the MPF's behave nearly periodically over a 90º rotor displacement, but the force distribution f^{α} is not exactly equal to the force distribution $f^{(\alpha-90^{\circ})}$ since the flux vector (with angle φ) slowly shifts relative to the rotor reference axis (with angle α) due to the slip $s \ll 1$:

$$\varphi = \frac{\alpha}{1-s} . \tag{10}$$

Consider an initial position where the flux is aligned with both a stator tooth and a rotor tooth. This initial position occurs for $\varphi=0$ and $\alpha=0$. The period of the MPF's is determined by the next full alignment between the flux, a rotor

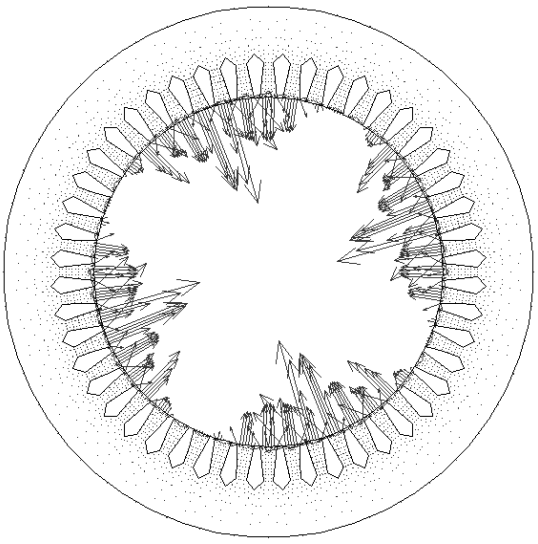

Fig.2 Force distribution acting on the stator teeth for rotor position $\alpha=20^{\circ}$ calculated using (8).

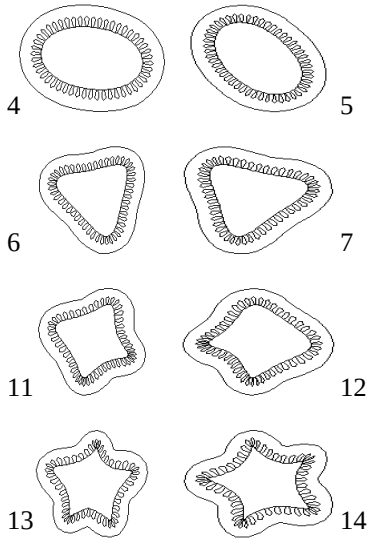

Fig.3 Several low-frequency mode shapes for the induction machine stator.

tooth and a stator tooth. The flux aligns with a rotor tooth for

$$\varphi - \alpha = k_1 \frac{360^\circ}{N_r} = k_1 10^\circ , \tag{11}$$

where N_r=36 is the number of rotor teeth and $k_1 \in$ Z. The flux aligns with a stator tooth for

$$\varphi = k_2 \frac{360^\circ}{N_s} = k_2 7.5^\circ , \tag{12}$$

where N_s=48 is the number of stator teeth and $k_2 \in$ Z. Starting from $\varphi=\alpha=0$, conditions (11) and (12) are satisfied for the first time for α=7500º or 20.83 revolutions. This fixes the period of the MPF's to 0.846 seconds. For 2º samples, 3750 field solutions are needed to cover this interval, resulting in a very large amount of CPU time and disk space. Judging from Fig.4 however, it is possible to approximate the period of the MPF's by 90º/(1–*s*)=88.66º or a multiple of this. Here, the period of the MPF's is approximated by 360º/(1–*s*)=354.6º. For 2º samples and using 5 minutes of CPU time per solution, this amounts to 15 hours of CPU time on a HP J2-240 workstation.

MODAL DECOMPOSITION

The vibration of the stator is governed by the global equation of motion

$$M_m \ddot{u} + C_m \dot{u} + Ku = f(t) , \tag{13}$$

where $u(t)$ is the nodal displacement and $f(t)$ is the force distribution acting on the stator, $f(t)= f^{\alpha}$ for $\alpha=2\pi nt/60$ (n=1478 rpm). M_m, C_m and K are the mechanical mass, damping and stiffness matrices respectively. Using the modal decomposition

$$u = Pq , \tag{14}$$

with P the modal matrix containing a selected set of N stator mode shapes and q the vector of generalized modal co-ordinates. Here P consists of the 30 modes with lowest eigenfrequency (N=30). Substituting (14) in (13) and premultiplying by P^T gives

$$P^T M_m P\ddot{q} + P^T C_m P\dot{q} + P^T KPq = P^T f(t) . \tag{15}$$

Only when the mechanical damping C_m is assumed to be proportional ($C_m=\alpha K+\beta M_m$), the system of equations (13) can be decoupled into [7]

$$\ddot{q}_i + 2\zeta_i \omega_i \dot{q}_i + \omega_i^2 q_i = \Gamma_i(t) , \; i = 1..N, \tag{16}$$

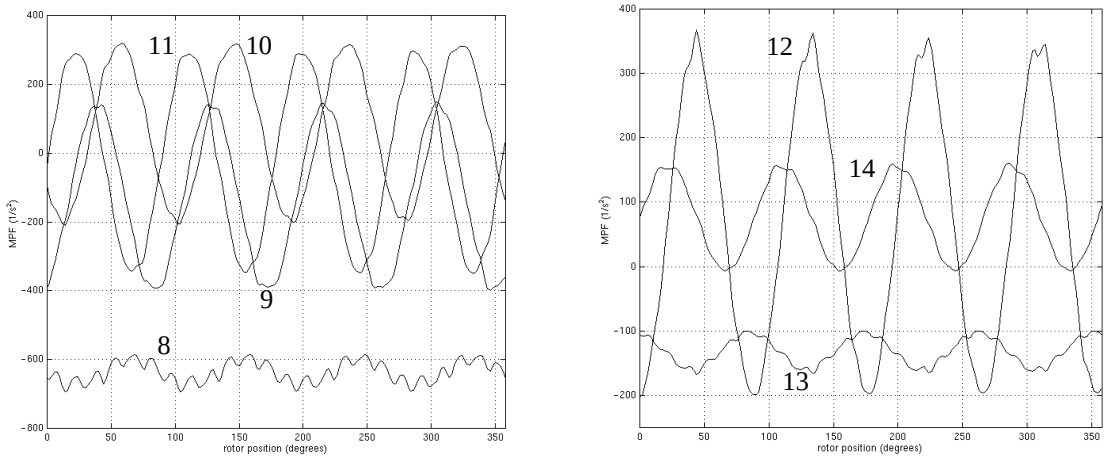

Fig.4 Mode participation factors for several modes as a function of rotor position (0<α<360º).

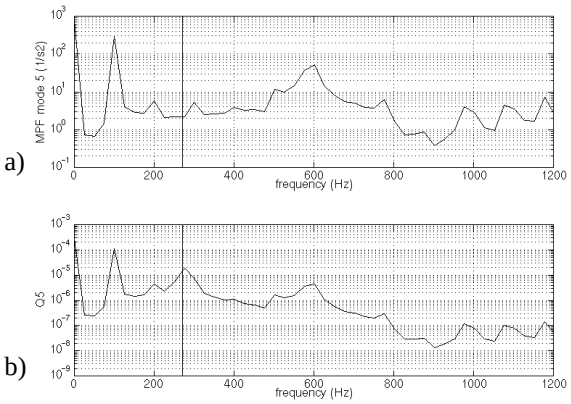

Fig.5

a) Spectrum of mode participation factor for mode 5,
b) Spectrum of modal co-ordinate for mode 5.

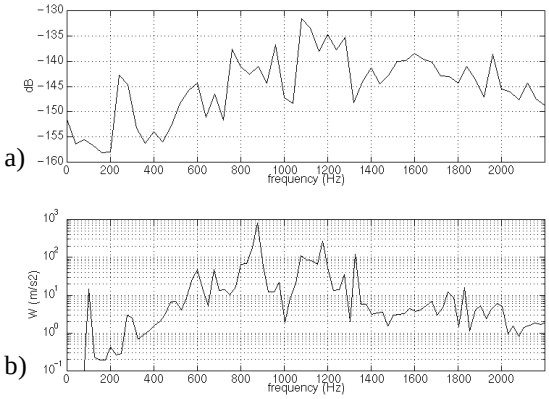

Fig.6

a) Measured spectrum for single stator location,
b) Computed spectrum at the same stator location.

where ω_i is the mode's angular eigenfrequency and ζ_i is the modal damping factor. Here damping is neglected (ζ_i=0). Note that the modal decomposition indeed transforms the force $f(t)$ into the MPF $\Gamma_i(t)$, $i = 1..N$, as prescribed by (9). From (9), the MPF's are known as a function of rotor position, so the rotor speed n allows us to find the MPF's as a function of time. The individual modal equations (16) are solved in the frequency domain after applying a discrete Fourier transformation to $q_i(t)$ and $\Gamma_i(t)$, giving the following relation between $Q_i(k\Delta\omega)$ and $G_i(k\Delta\omega)$:

$$Q_i(k\Delta\omega) = \frac{G_i(k\Delta\omega)}{\omega_i^2 - (k\Delta\omega)^2}\,. \tag{17}$$

Fig.5a shows, in semi-log scale, the discrete amplitude spectrum $G_5(k\Delta f)$ of the MPF of the 5th mode with eigenfrequency f_5=268 Hz (indicated by the vertical line). Fig.5b shows the corresponding amplitude spectrum $Q_5(k\Delta f)$ of the generalized co-ordinate $q_5(t)$ calculated using (17). The higher frequency components are attenuated more than the lower frequency components and around f_5, there is a local amplification of the response of this mode. The spectrum of any individual mode shape can be found as described above. The separated complex spectra Q_i of the relevant modes are composed again into the actual stator displacement spectra U using the modal composition (14).

VIBRATION MEASUREMENTS

The displacement spectra $U(k\Delta\omega) = P\,Q(k\Delta\omega)$ are first converted into acceleration spectra $W(k\Delta\omega)$ in order to compare the simulations with accelerometer measurements on the surface of the induction motor stator:

$$W(k\Delta\omega) = -(k\Delta\omega)^2\,U(k\Delta\omega)\,. \tag{18}$$

Fig.6a shows the acceleration spectrum measured at a single point on the surface of the stator. Fig.6b shows the corresponding acceleration spectrum of this point calculated using the method described above. Although there is a good coincidence between the measured and calculated spectrum, the accuracy of the numerical prediction is limited. The mode shapes are calculated taking only the iron yoke and copper coils into account, but neglecting the

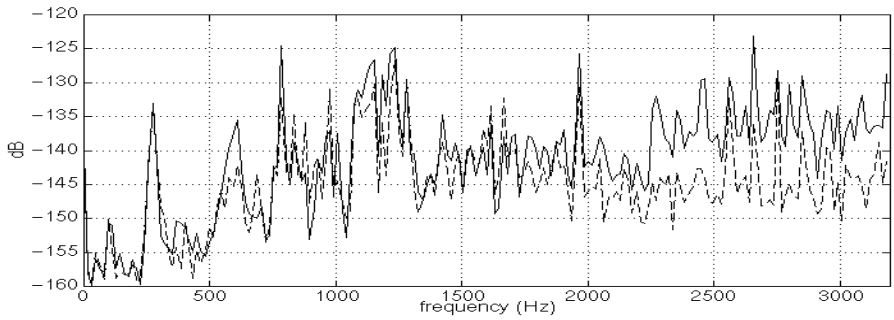

Fig.7 Acceleration spectra of stator points at different locations along the axial direction.

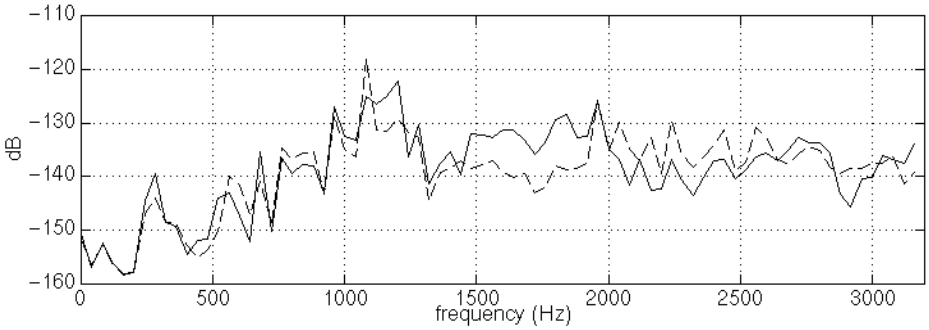

Fig.8 Acceleration spectra of two points on machine mounting.

end caps, the aluminum motor frame, the connecting box and the cooling fins. No material or structural damping is considered. A less important source of error is the approximation of the periodicity of the MPF. To obtain a more accurate predicted spectrum, the mechanical model needs to be expanded with (some of) these features.

A 3D mechanical model will produce a higher modal density [8] and thus a higher response to a given force excitation. This effect can be seen from Fig.7. Here two spectra measured for different locations on the stator surface are compared. These locations differ in their *axial* position only and are represented by the same 2D co-ordinates. The spectra remain fairly equal up to 2000 Hz, indicating the domination of 2D modes in this frequency range. For higher frequencies, 3D modes start playing an important role and the spectra differ more and more. Therefore, predictions based on 2D mode shapes are restricted to the low-frequency range.

Accelerometers are also positioned on the mountings of the induction machine. The resulting spectra are shown in Fig.8. The spectrum of the mountings is of the same order of magnitude as the spectra of points on the stator surface. From this it can be concluded that there is no important accuracy gain by incorporating the (theoretically) rigid mountings into the mechanical model, e.g. to calculate the mode shapes.

CONCLUSIONS

Using 2D mechanical and magnetic finite element models, a numerical prediction of the vibration spectrum of the 45 kW induction machine is obtained. The force distribution occurring for all relevant rotor positions is correlated to the 2D mode shapes of the induction machine stator, yielding *mode participation factors* as a function of time. A finite element expression for local electromagnetic reluctance forces is presented. The global equation of motion of the stator is decomposed into modal equations of motion which are solved separately in the frequency domain. The spectral information of the modes is transformed back into spectral acceleration information for the stator surface.

Considering the restriction to 2D models, a good agreement is obtained between predicted and measured vibration spectra. The full analysis required 15 hours of CPU time. Better predictions will require the use of 3D mechanical models incorporating the end-caps.

ACKNOWLEDGMENT

The authors are grateful to the Belgian "Fonds voor Wetenschappelijk Onderzoek Vlaanderen" for its financial support; Koen Delaere has a FWO-V scholarship. The authors thank the Belgian Ministry of Scientific Research for granting the IUAP No.P4/20 on Coupled Problems in Electromagnetic Systems. The research Council of the K.U.Leuven supports the basic numerical research. Special thanks to R.Mertens for his valuable help in preparing the FE models.

REFERENCES

1. O.C. Zienkiewicz, R.L. Taylor, *The Finite Element Method* (McGraw-Hill, 1989)
2. P.P. Silvester, R.L. Ferrari, *Finite Elements for Electrical Engineers, Third Edition* (Cambridge University Press, 1996)
3. "Finite element implementation of virtual work principle for magnetic or electric force or torque computation," J.L. Coulomb, G. Meunier, *IEEE Transactions on Magnetics,* **20** no.5, 1894–1896 (1984)
4. "Local force computation in deformable bodies using edge elements," Z. Ren, A. Razek, *IEEE Transactions on Magnetics*, **28**, 1212–1215 (1992)
5. J.T. Oden, *Mechanics of Elastic Structures* (McGraw-Hill, 1967)
6. W.T. Thomson, *Theory of Vibrations with Applications, Fourth Edition* (Prentice-Hall, 1993)
7. L. Meirovich, *Computational Methods in Structural Dynamics* (Sijthoff & Noordhoff, 1980)
8. "An acoustic model for a permanent magnet machine: modal shapes and magnetic forces," D. Verdyck, R. Belmans, *IEEE Transactions on Industry Applications (IAS)*, **30** no.6, 1625–1631 (1994)